Journal of Transportation Technologies, 2026, 16(2), 274-296
https://www.scirp.org/journal/jtts
ISSN Online: 2160-0481
ISSN Print: 2160-0473

Dynamic Biofouling Risk Assessment for Ships Using AIS Data and Environmental Factors

Hourong Song[1], Feiyang Ren[2], Yingchao Gou[3*]

[1]Department of Science, Technology and Innovation, COSCO Shipping Bulk Co., Ltd., Guangzhou, China
[2]Research and Development Innovation Center, COSCO Shipping Technology Co., Ltd., Shanghai, China
[3]School of Ocean & Civil Engineering, Shanghai Jiao Tong University, Shanghai, China
Email: hourong@coscoshipping.com, ren.feiyang@coscoshipping.com, *gyczbl@sjtu.edu.cn

How to cite this paper: Song, H.R., Ren, F.Y. and Gou, Y.C. (2026) Dynamic Biofouling Risk Assessment for Ships Using AIS Data and Environmental Factors. *Journal of Transportation Technologies*, **16**, 274-296.
https://doi.org/10.4236/jtts.2026.162016

Received: March 9, 2026
Accepted: April 4, 2026
Published: April 7, 2026

Copyright © 2026 by author(s) and Scientific Research Publishing Inc.
This work is licensed under the Creative Commons Attribution International License (CC BY 4.0).
http://creativecommons.org/licenses/by/4.0/

Open Access

Abstract

Marine biofouling on ship hulls poses a dual challenge to the global shipping industry, leading to significant penalties in hydrodynamic performance and increasing the risk of invasive aquatic species (IAS) transfer. Traditional biofouling management relies heavily on fixed-interval maintenance or reactive cleaning based on visible speed loss, which lacks precision and often fails to address the dynamic nature of biological growth. This study proposes a novel, data-driven framework for assessing biofouling risk by integrating high-frequency Automatic Identification System (AIS) kinematic data with spatiotemporal environmental exposure parameters. The model quantifies risk through a multi-factor index that accounts for vessel downtime, sea surface temperature, and traversal of ecologically sensitive geographic zones. A case study involving a coastal bulk carrier and a global ocean-going vessel was conducted to validate the framework. Results demonstrate that the model can effectively distinguish between static-driven fouling risks in coastal operations (dominated by 94% slow-flow events) and metabolic-driven risks in global operations (dominated by 44% high-temperature exposure). The system achieved a classification accuracy of approximately 87% against a validation dataset, with a 100% detection rate for entries into known high-risk estuarine areas. By transforming abstract biological pressures into a quantifiable engineering metric, this research provides ship operators with a proactive decision-support tool to optimize hull cleaning schedules, thereby enhancing fuel efficiency and ensuring compliance with emerging environmental regulations such as the IMO's Carbon Intensity Indicator (CII).

Keywords

Marine Biofouling, Biofouling Risk Assessment, AIS Data, Ship Hull Performance, Invasive Aquatic Species, Condition-Based Maintenance

1. Introduction

Maritime transportation underpins over 90% of global trade by volume, serving as the lifeblood of international supply chains while facing unprecedented pressure to decarbonize [1] [2]. The International Maritime Organization (IMO) has set ambitious targets to reduce greenhouse gas (GHG) emissions by at least 50% by 2050 compared to 2008 levels, with a long-term vision of net-zero emissions [3]. However, ship biofouling—defined as the undesirable accumulation of microorganisms, algae, barnacles, and other marine organisms on submerged hull surfaces—poses a critical barrier to achieving these goals. By increasing hull roughness and hydrodynamic resistance, biofouling can raise fuel consumption by 10% - 86% and corresponding GHG emissions, depending on the fouling type and severity [4]-[6]. Beyond economic and climate impacts, biofouling is responsible for introducing approximately 55% of non-indigenous marine species (NIS) globally, threatening marine biodiversity and ecosystem stability through biological invasion [7] [8]. It also contributes to environmental pollution via biocidal coating leaching and hull-cleaning effluents, further exacerbating marine ecosystem pressures [9] [10].

Effective antifouling cleaning and maintenance are key to mitigating these risks, but their success hinges on scientific risk assessment that balances cleaning costs, operational efficiency, and environmental impacts [11]. Over the past two decades, research on ship biofouling risk assessment has evolved to address multiple risk dimensions, including operational economics, climate impacts, biological invasion, and environmental pollution [8] [12]. Existing studies have identified core influencing factors spanning environmental conditions (water temperature, salinity, nutrient availability), vessel characteristics (ship age, hull coating type, maintenance cycle), and navigation behaviors (duration of navigation suspension, water area exposure characteristics) [2] [13]. These factors form the basis of three main categories of assessment models: physical models (PMs), data-driven models (DDMs), and hybrid models (HMs) [2]. Physical models, such as computational fluid dynamics (CFD) simulations and Granville's boundary layer similarity law, rely on mechanistic knowledge to quantify fouling-induced resistance and power losses [14] [15]. Data-driven models, leveraging machine learning algorithms (e.g., artificial neural networks, random forests), use operational data (e.g., AIS trajectories, fuel consumption records) to predict fouling impacts without requiring detailed physical insights [11] [16]. Hybrid models, which integrate physical principles with data-driven approaches, have emerged as a promising direction to overcome the computational complexity of PMs and the lack of physical interpretability in DDMs, though their application to biofouling assessment remains limited [2] [11].

Parallel to model development, geographical risk assessment has gained attention as biofouling severity is highly dependent on spatial and environmental contexts. Studies have identified high-risk biofouling waters, including tropical/subtropical ports, nutrient-rich river estuaries, and slow-flow anchorage areas, where warm temperatures, abundant nutrients, and reduced water movement facilitate

organism growth. Early geographical risk frameworks primarily relied on broad latitudinal zoning or static port categorization, but recent advances have incorporated GIS-based spatial analysis to map fouling hotspots [17] [18]. Additionally, policy and regulatory developments (IMO Biofouling Guidelines, 2011, 2023) and regional regulations in California, New Zealand, and the Baltic Sea have emphasized risk-based management, further driving the need for refined assessment tools that align with operational decision-making.

Despite the clear necessity for effective biofouling management, current industrial practices remain largely reactive or heuristic. The traditional approach relies on calendar-based dry-docking intervals (typically every 30 to 60 months) or periodic underwater inspections triggered only when a vessel exhibits significant speed loss or fuel overconsumption. This "fail-and-fix" strategy is inherently inefficient. It often leads to either premature cleaning operations that damage antifouling coatings or delayed interventions that allow hard fouling to establish, necessitating aggressive cleaning methods that release biocides and microplastics into the marine environment. Existing academic research has made strides in modeling biofouling growth, primarily through laboratory-based experiments or Computational Fluid Dynamics (CFD) simulations of roughness effects. However, there is a notable disconnect between these theoretical models and the operational reality of commercial shipping. Most existing models treat biofouling as a function of time, neglecting the critical influence of the vessel's specific operational profile, where it sails, how long it stays idle, and the environmental conditions it encounters. For instance, a vessel idling for two weeks in a tropical estuary faces a vastly higher fouling pressure than a vessel constantly steaming in cold, open ocean waters. Current risk assessment tools often lack the granularity to capture these spatiotemporal variations, failing to leverage the massive volume of kinematic data available through the Automatic Identification System (AIS) to create dynamic, vessel-specific risk profiles.

To address these critical gaps, this study aims to develop a quantitative and practical ship biofouling risk assessment method tailored to operational needs. The objective focuses on three areas. First, the study defines precise latitudinal and longitudinal boundaries for high-risk biofouling waters to enable accurate exposure detection. Second, it proposes a daily count-based downtime quantification method that simplifies calculations and aligns with vessel management practices. Third, the research constructs a multi-dimensional risk assessment model integrating six core factors, including downtime characteristics, geographic risk exposure, typical water exposure, inspection overdue status, and vessel age, to generate a continuous risk score. By fusing AIS trajectory data with marine environmental and vessel attribute data, the proposed method overcomes the limitations of traditional qualitative assessment approaches. The contributions of this work are significant. It introduces a percentage-based scoring system that fills the gap in quantitative biofouling assessment and supports data-driven maintenance decisions. The daily count-based downtime method resolves the disconnection between statistical models and operational reality, offering a user-friendly metric for planning. Furthermore, the inte-

grated framework combines spatial point-in-polygon detection with multi-factor weighting to provide a holistic view of biofouling risk. This approach effectively bridges the divide between academic research and industrial application. Practically, the method empowers shipping companies to optimize cleaning schedules, reduce fuel costs, and minimize environmental impacts while supporting maritime authorities in implementing refined biosecurity measures.

The remainder of this paper is organized as follows. Section 2 details the methodology, including high-risk water definition, data preprocessing, risk factor quantification, and the multi-dimensional percentage model. Section 3 presents empirical results using actual vessel data to verify the method's validity. Section 4 discusses the scientificity, practicality, and limitations of the approach. Finally, Section 5 summarizes the main conclusions and proposes future research directions.

2. Methodology

2.1. Overall Assessment Framework and Definition of High-Risk Biofouling Waters

This study proposes a ship biofouling risk assessment system, designed to realize quantitative and refined risk evaluation for supporting antifouling cleaning decisions. The overall framework of the system is illustrated in Figure 1, which consists of four functional modules: 1) geographical risk assessment, 2) downtime quantification, 3) percentage risk calculation, and 4) risk grading-alarm generation. The modules are logically connected with data transmission and factor fusion, taking ship trajectory, marine weather, and ship basic data as input, and outputting total risk percentage, risk grade, early warning information, and targeted antifouling suggestions.

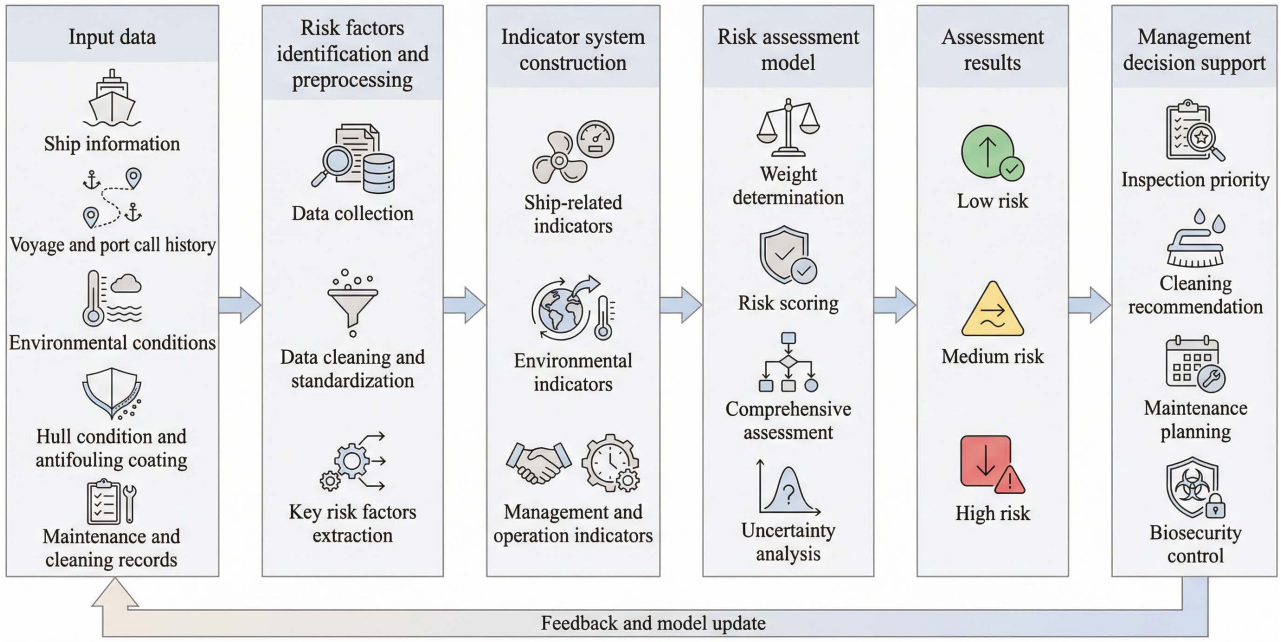

Figure 1. Overall framework of the ship biofouling risk assessment system.

Table 1. Classification and characteristics of high-risk biofouling waters (HRBW).

HRBW Category	Environmental Characteristics	Typical Representative Ports	Geographical Boundary Method
Tropical/Subtropical Ports	High water temperature (>25˚C), stable hydrological conditions	Singapore Port, Laem Chabang Port, Jebel Ali Port	Latitude-longitude polygon
Temperate Waters (Summer)	Seasonally high water temperature, abundant sunlight	Yangshan Port, Ningbo-Zhoushan Port, Piraeus Port	Latitude-longitude polygon
River Estuaries (Rich in Nutrients)	High nutrient salt content, slow water exchange	Yangtze River Estuary, Pearl River Estuary, Mississippi River Mouth	Latitude-longitude polygon
Slow-Flow Waters	Extremely low flow velocity, poor water mobility	Suez Canal Anchorage, Panama Canal Anchorage, Tokyo Bay	Latitude-longitude polygon

Biofouling organisms' growth and reproduction are highly dependent on marine environmental factors such as water temperature, nutrient salt content, and water flow velocity [4]. Based on the growth law of typical biofouling organisms (e.g., barnacles, algae) and engineering practice of maritime operations, four categories of high-risk biofouling waters (HRBW) are defined in this study, and each category is characterized by specific geographical and environmental features that facilitate biofouling. The division of HRBW and their typical representative ports are summarized in Table 1. To precisely define these areas and ensure the reproducibility of geographic risk evaluations, the exact latitude and longitude bounding-box coordinates for all 19 specific zones are provided in **Appendix** Table A1. This supplementary spatial data explicitly delineates the geographic boundaries of each HRBW category.

2.2. Data Acquisition and Preprocessing

2.2.1. Data Sources and Key Parameters

Three types of data were collected as the research foundation, covering ship operation characteristics, marine environmental conditions, and ship inherent attributes. All data were selected with a time range from 2022-01-01 to 2025-12-31, and the key fields and physical meanings of each dataset are as follows:

- Ship trajectory data: Collected from the automatic identification system (AIS) of ships, with the core identifier of maritime mobile service identity (MMSI). The data was provided by COSCO Shipping Technology Co., Ltd. Key fields include AIS posting time, speed over ground (SOG) (knots), longitude (lon, ˚) and latitude (lat, ˚), draught (m), start/end port code, destination port, and estimated time of arrival (ETA).
- Marine weather data: Acquired from the National Data Buoy Center (NDBC) of NOAA, a publicly accessible global marine environmental monitoring database. The raw granularity is 6 hours per record. Key fields include water temperature (watertemp, ˚C), swell height (m), swell direction (˚), swell period (s), course over ground (COG) (˚), and heading (HDG) (˚). Water temperature is the core environmental factor for biofouling assessment, and other hydrological parameters are used as auxiliary supplements.

- Ship basic data: Obtained from the ship management database of COSCO Shipping Technology Co., Ltd., including MMSI, international maritime organization (IMO) number, ship type, build year, and maintenance history (survey date, survey type). This data provides inherent attribute parameters for risk assessment, such as ship age and inspection cycle.

2.2.2. Data Preprocessing

To ensure the validity and consistency of data input for the risk assessment model, three preprocessing steps were implemented for the original datasets, following the general data processing principles for maritime engineering research.

Missing values of key numerical fields (e.g., SOG, watertemp, lon/lat) were filled with the mean value of adjacent time series; records with missing core identifiers (MMSI) or spatial coordinates (lon/lat) were deleted directly. Abnormal values were identified and eliminated using the 3σ principle, where values beyond the range of $\mu \pm 3\sigma$ (μ = mean, σ = standard deviation) were regarded as abnormal. Duplicate records based on MMSI and AIS posting time were removed to ensure data uniqueness.

The 6-hour granular marine weather data was aggregated into daily average values by grouping with MMSI and date, to match the time granularity of ship trajectory data and avoid temporal mismatch in subsequent data fusion. All weather metrics (e.g., watertemp, swell height) were calculated using the arithmetic mean for daily aggregation.

Ship trajectory data and aggregated weather data were merged by a left join on MMSI and date, generating an integrated dataset that fuses ship navigation characteristics and marine environmental conditions. For missing start/end port codes in the trajectory data, a lag filling method was adopted: the end port code of the previous navigation segment was used to fill the missing start port code of the current segment, ensuring the integrity of route information for subsequent geographical risk tracing.

The spatial matching between marine weather data and vessel positions was implemented using a nearest-grid-point method. For each AIS position record, the system identified the nearest grid cell in the global marine weather dataset (sourced from NDBC/NOAA) based on the geodetic distance between the vessel's longitude-latitude coordinates and the grid cell centers. The weather dataset provides global ocean coverage with a spatial resolution of approximately $0.5^\circ \times 0.5^\circ$, ensuring that each vessel position can be matched to a corresponding environmental observation. The temporal alignment was achieved by matching each daily AIS record to the daily-averaged weather value (aggregated from the original 6-hour granularity records) on the same date. This nearest-grid-point approach achieved a coverage rate of over 95% across all vessel-days in the study period, with the remaining gaps primarily occurring in polar or sparsely monitored waters outside the vessels' operational areas. Days without matched weather data were excluded from the typical water exposure calculation to avoid introducing bias.

2.3. Quantification of Key Biofouling Risk Factors

Two types of risk factors (geographical risk exposure and ship downtime) were quantified in this study, which are the most direct and important factors affecting ship biofouling [18]. The quantification methods were designed to be consistent with maritime operation practices, with refined identification and simplified calculation to balance assessment accuracy and engineering applicability.

2.3.1. Geographical Risk and Typical Water Area Exposure Quantification

A typical water exposure point (TWP) is defined as an AIS position record at which the vessel is exposed to environmental conditions conducive to biofouling organism growth. Specifically, an AIS record is classified as a TWP if it satisfies at least one of the following criteria:

1) The sea surface temperature (SST) at the vessel's position exceeds 15˚C, which corresponds to the lower thermal threshold for accelerated growth of common hard-fouling taxa such as barnacles (*Balanus* spp.) and tubeworms (*Hydroides* spp.) [4];

2) The vessel's speed over ground (SOG) is below 5.0 knots, indicating slow transit through waters where fouling organisms have sufficient time to initiate settlement on the hull surface.

The typical water area count (TWC) is defined as the total number of TWPs accumulated within a given assessment period:

$$TWC = \left|\{p \in \text{AIS records} \mid SST(p) > 15^{\circ}C \text{ or } SOG(p) < 5.0 \text{ kn}\}\right|. \quad (1)$$

where p denotes an individual AIS position record, SST(p) denotes the sea surface temperature at record p, SOG(p) denotes the speed over ground at record p, $|\cdot|$ denotes the cardinality of a set representing the total number of elements.

Geographical risk assessment was implemented based on the pre-defined HRBW (**Table 1**) and a point-in-polygon geometric detection method, which is a classic spatial analysis method for geographic risk identification. For each ship trajectory point $P(\text{lon}, \text{lat})$ in the integrated dataset, the detection principle is defined as:

$$Contains(P, Polygon) = \begin{cases} True, if\ P \in Polygon\ or\ P\ touches\ Polygon \\ False, otherwise \end{cases}, \quad (2)$$

where Polygon is the latitude-longitude polygon of a specific HRBW category (**Table 1**), if the detection result is True, the point is identified as an HRBW exposure point; the total number of such points in the assessment period is defined as geographic risk count (GRC), a quantitative index for subsequent risk calculation. Route information (start/end port code, route description) was attached to each HRBW exposure point to realize refined tracing of geographical risk sources.

2.3.2. Vessel Downtime Quantification Based on Daily Count

Ship downtime is a critical factor for biofouling, as biofouling organisms are more likely to attach to the hull when the ship is stationary or moving at an ultra-low speed [11]. A practical downtime quantification method based on daily count was

proposed in this study, which is adapted to the actual scenario of "daily decision-making" in ship management and maintenance, avoiding the complexity of cross-day calculation in traditional hour-level downtime statistics.

Table 2. Quantification indicators of ship downtime based on daily count.

Indicator Name	Abbreviation	Symbol Explanation	Physical Meaning
Total Downtime Days	TDD	$d \in D \mid \exists r \in R(d), SOG(r) < 2.5$, where D is the assessment date set; R (d) represents the ship trajectory record set on date d	Number of unique days with downtime records in the assessment period
Risk Area Downtime Days	RADD	$d \in TDD \mid \exists r \in R(d), SOG(r) < 2.5 \cap r \in H$, where H means high-risk biofouling waters (HRBW) exposure record set	Number of unique downtime days in the pre-defined HRBW
Non-Risk Area Downtime Days	NRADD	NRADD = TDD − RADD	Number of unique downtime days in non-HRBW waters (auxiliary assessment indicator)

The downtime judgment criterion was defined as SOG < 2.5 knots, which is consistent with the industry standard for identifying ship berthing and anchoring states [11]. Based on this criterion, three downtime indicators were quantified with the assessment period days (APD) as the time reference, where APD is the total number of days from the start date to the end date of the assessment period. The definitions, formulas, and physical meanings of the downtime indicators are summarized in Table 2.

2.4. Multi-Dimensional Percentage Risk Assessment Model

A multi-dimensional percentage risk assessment model was established as the core of this study, which integrates navigation characteristics, ship inherent attributes, and environmental factors to calculate the total biofouling risk percentage (TRP) of ships (0% - 100%). The model adopts a weighted scoring method for six core assessment indicators, with clear calculation formulas and normalized processing to ensure the scientificity and repeatability of the assessment results. After calculating TRP, a risk grading standard and an early warning mechanism were designed to connect quantitative assessment results with practical antifouling cleaning decisions.

2.4.1. Selection and Weighting of Assessment Indicators

Six assessment indicators were selected, covering three dimensions of biofouling influence factors: navigation characteristic indicators (typical water area count (TWC), GRC, TDD, RADD), ship inherent attribute indicators (months since inspection (MSI), Ship age (SA)). The weight and scoring interval of each indicator were determined by combining expert experience and maritime engineering practice, where the scoring interval represents the maximum contribution of each indicator to the total risk percentage (0% - 100%). The complete indicator system is summarized in Table 3, with the physical meaning of each indicator clearly ex-

plained.

Table 3. Indicator system for ship biofouling risk assessment (weighted scoring).

Indicator Dimension	Indicator Name	Abbreviation	Scoring Interval (%)	Physical Meaning
Navigation characteristic	Total Downtime Days	TDD	0 - 30	Reflects the overall downtime degree of the ship in the assessment period
Navigation characteristic	Risk Area Downtime Days	RADD	0 - 15	Reflects the downtime degree in HRBW (additional risk score)
Navigation characteristic	Geographic Risk Count	GRC	0 - 25	Reflects the frequency of ships passing through HRBW
Navigation characteristic	Typical Water Area Count	TWC	0 - 20	Reflects the frequency of ship exposure to typical biofouling water areas
Ship inherent attribute	Months Since Inspection	MSI	0 - 15	Reflects the overdue degree of ship maintenance and antifouling inspection
Ship inherent attribute	Ship Age	SA	0 - 10	Reflects the influence of hull aging on biofouling resistance

The SOG threshold of 2.5 knots for downtime identification is consistent with the widely adopted industry practice for distinguishing between navigating and stationary vessel states [11]. This threshold is also recommended in the IMO Guidelines for the Control and Management of Ships' Biofouling (IMO, 2011) as an indicator of conditions where hull fouling accumulation is significantly accelerated. The temperature-based risk threshold of 15˚C is grounded in marine biology literature, as this value represents the approximate lower thermal limit above which the growth rate of major fouling organisms (including barnacles, bryozoans, and algae) increases substantially [6] [19]. Below this temperature, biofouling growth is generally slow enough to pose minimal operational risk within typical inter-cleaning intervals.

The relative weights assigned to the six assessment indicators (**Table 3**) were determined through a structured expert elicitation process. Five industry professionals from COSCO Shipping Technology Co., Ltd. and COSCO Shipping Bulk Co., Ltd., each with over 10 years of experience in vessel hull maintenance, antifouling management, and fleet operations, independently assigned importance scores to each indicator. The final weights represent the consensus allocation after two rounds of discussion using a modified Delphi approach. The resulting weight structure reflects the expert consensus that vessel downtime (combined DRS + RDRS weight: 45%) and geographical/environmental exposure (combined GRS + TES weight: 45%) are the dominant drivers of biofouling accumulation, while ship-intrinsic factors (IRS + ARS: 25%) provide baseline risk modulation. This allocation is consistent with the findings of Luoma *et al.* (2022), who identified operational exposure and environmental conditions as the primary determinants of hull fouling severity.

2.4.2. Calculation of Sub-Item Risk Scores and Total Risk Percentage

All six assessment indicators were normalized and weighted to calculate the sub-item risk scores, with the calculation results limited to the corresponding scoring intervals (Table 3) to avoid excessive contribution of a single indicator to the total risk. The sub-item risk score of each indicator was calculated using the formulas below (Equations (3) - (8)), and all symbols were first defined with APD as the unified time reference for normalization.

1) Downtime risk score (DRS) (0% - 30%):

$$\mathrm{DRS} = \min\left(\frac{\mathrm{TDD}}{\mathrm{APD}}, 1.0\right) \times 30, \tag{3}$$

where $\frac{\mathrm{TDD}}{\mathrm{APD}}$ is the downtime ratio; the $\min(\cdot, 1.0)$ function limits the maximum downtime ratio to 100% to avoid over-scoring.

2) Risk area downtime risk score (RDRS) (0% - 15%):

$$\mathrm{RDRS} = \min\left(\frac{\mathrm{RADD}}{\mathrm{APD}}, 1.0\right) \times 15. \tag{4}$$

3) Geographic risk score (GRS) (0% - 25%):

$$\mathrm{GRS} = \min\left(\frac{\mathrm{GRC}}{\mathrm{APD}/30}, 1.0\right) \times 25, \tag{5}$$

where $\frac{\mathrm{GHC}}{\mathrm{APD}/30}$ is the monthly frequency of HRBW exposure (converted by APD/30), reflecting the long-term geographical risk of the ship.

4) Typical exposure score (TES) (0% - 20%):

$$\mathrm{TES} = \min\left(\frac{\mathrm{TWC}}{\mathrm{APD}/7}, 1.0\right) \times 20, \tag{6}$$

where $\frac{\mathrm{TWC}}{\mathrm{APD}/7}$ is the weekly frequency of typical water area exposure (converted by APD/7), reflecting the frequent exposure to biofouling-conducive waters.

5) Inspection risk score (IRS) (0% - 15%):

$$\mathrm{IRS} = \min\left(\frac{\mathrm{MSI}}{\mathrm{IC}} \times 7.5, 15\right), \tag{7}$$

where IC is the inspection cycle (months); the IC is determined by ship type and SA: IC = 30 months for container ships or ships with $\mathrm{SA} \geq 10$ years, and $\mathrm{IC} = 60$ months for other ships. $\frac{\mathrm{MSI}}{\mathrm{IC}}$ is the inspection overdue ratio, with a maximum score limited to 15%.

6) Age risk score (ARS) (0% - 10%):

$$\mathrm{ARS} = \min\left(\frac{\mathrm{SA}}{20} \times 10, 10\right), \tag{8}$$

where SA is the ship age (years, calculated as the research year minus the build year); the formula is based on the industry consensus that the hull's biofouling

resistance decreases significantly after 20 years of service, with a maximum score limited to 10%.

The total biofouling risk percentage (TRP) was calculated as the sum of all six sub-item risk scores, with the result limited to the range of 0% - 100% to ensure the rationality of the quantitative assessment result:

$$\mathrm{TRP} = \mathrm{DRS} + \mathrm{RDRS} + \mathrm{GRS} + \mathrm{TES} + \mathrm{IRS} + \mathrm{ARS},\ \mathrm{TRP} \in [0,100] \tag{9}$$

2.4.3. Risk Grade Classification and Early Warning Mechanism

Based on the TRP value, a five-level risk grading standard was designed to match the practical needs of antifouling cleaning decision-making. The risk grading standard is summarized in Table 4, which is the direct basis for converting quantitative TRP values into qualitative risk grades.

An early warning message generation mechanism was further established by combining the risk grade (Table 4) with key risk factors (e.g., MSI > IC, RADD > 15, GRC > 0). The early warning messages are divided into four types according to the risk level: normal alert (risk grade: extremely low), prompt alert (passing through HRBW/typical water areas), warning alert (long downtime in HRBW), and emergency alert (inspection overdue + high/extremely high risk). Each type of early warning message contains specific risk factor descriptions and operable antifouling suggestions, realizing the integration of quantitative assessment, qualitative grading, and practical decision-making.

Table 4. Ship biofouling risk grade classification based on total risk percentage (TRP).

Risk Grade	TRP Range (%)	Antifouling Cleaning Decision Suggestions
Extremely Low	TRP < 15	No immediate cleaning required; regular hull inspection
Low	15 ≤ TRP < 30	Strengthen hull monitoring; plan cleaning in the next maintenance
Medium	30 ≤ TRP < 50	Schedule targeted cleaning within a short time (1 - 3 months)
High	50 ≤ TRP < 70	Immediate targeted cleaning; check hull antifouling coating
Extremely High	TRP ≥ 70	Urgent full hull cleaning; comprehensive maintenance of the antifouling system

3. Case Study

To validate the proposed biofouling risk assessment framework, a comprehensive case study was conducted using real-world vessel operation data. The study aims to demonstrate the system's capability in capturing distinct risk profiles across different operational patterns—ranging from short-haul coastal voyages to long-distance global navigation—and to evaluate the quantitative accuracy of the risk indexing mechanism.

3.1. Dataset and Experimental Setup

The experimental dataset consists of high-frequency AIS trajectories and environmental exposure records from two representative commercial vessels over a combined observation period spanning from January 2023 to August 2025. These vessels were selected to represent two divergent operational profiles common in the merchant fleet.

- Vessel A (coastal operator): A bulk carrier operating exclusively within Chinese coastal waters (Bohai Sea and Yellow Sea). The assessment period covers one full year (January 1, 2024, to January 1, 2025). This vessel frequently shuttles between domestic ports (e.g., Huaian Port, Dalian Port), characterized by short sea voyages and frequent port calls.
- Vessel B (global operator): A large bulk carrier/tanker engaged in global trade. The data covers two distinct phases: Period 1 (January 2023 to December 2024) and Period 2 (February 2025 to August 2025). Its routes traverse the Atlantic, Pacific, and Indian Oceans, visiting 31 ports across North America, Europe, South America, and Asia.

The system processed a total of 50 distinct routes and 38 unique port calls. For validation purposes, a supplementary labeled dataset consisting of 45 simulated vessel profiles over 120 assessment periods was generated to rigorously test the classification boundaries of the risk model.

The validation dataset was constructed as follows. First, 45 synthetic vessel operational profiles were generated by sampling realistic combinations of key parameters—including route type (coastal vs. global), total downtime duration, geographic risk zone exposure frequency, ship age, and inspection history—from the statistical distributions observed in the real operational dataset of Vessels A and B. Each synthetic profile was designed to represent a plausible assessment period scenario, covering the full spectrum from low-risk coastal operations to high-risk tropical voyages. The risk labels for all 120 assessment periods were then independently assigned by three domain experts from COSCO Shipping Technology Co., Ltd., each with over 10 years of professional experience in vessel hull maintenance, dry-docking inspection, and antifouling coating management. Each expert evaluated the synthetic profiles based on their professional judgment and assigned one of three risk categories (High, Medium, or Low). Inter-rater agreement was assessed using Fleiss' kappa, yielding $\kappa = 0.82$, indicating substantial agreement. Final labels were determined by majority vote. It should be explicitly noted that these validation labels represent expert-simulated risk judgments rather than observed hull-condition inspection outcomes.

3.2. Risk Characterization of Coastal Operations

Vessel A serves as a quintessential example of a coastal vessel subject to "stop-and-go" operational risks. The analysis identified 325 typical water exposure points during the one-year assessment window.

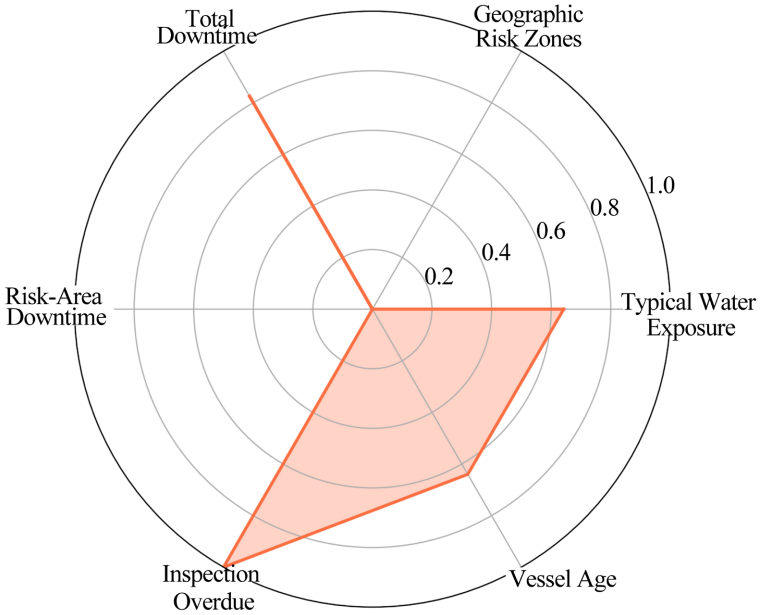

Figure 2. Six-dimensional biofouling risk profile.

Figure 2 presents the six-dimensional biofouling risk radar for vessel A. The profile is heavily skewed towards typical water exposure and total downtime, while geographic risk zones remain negligible. Detailed factorization reveals that slow flow events (port stays and anchoring) account for the vast majority of risk accumulation (307 hits), whereas high temperature events are secondary (135 hits), occurring primarily during the summer months.

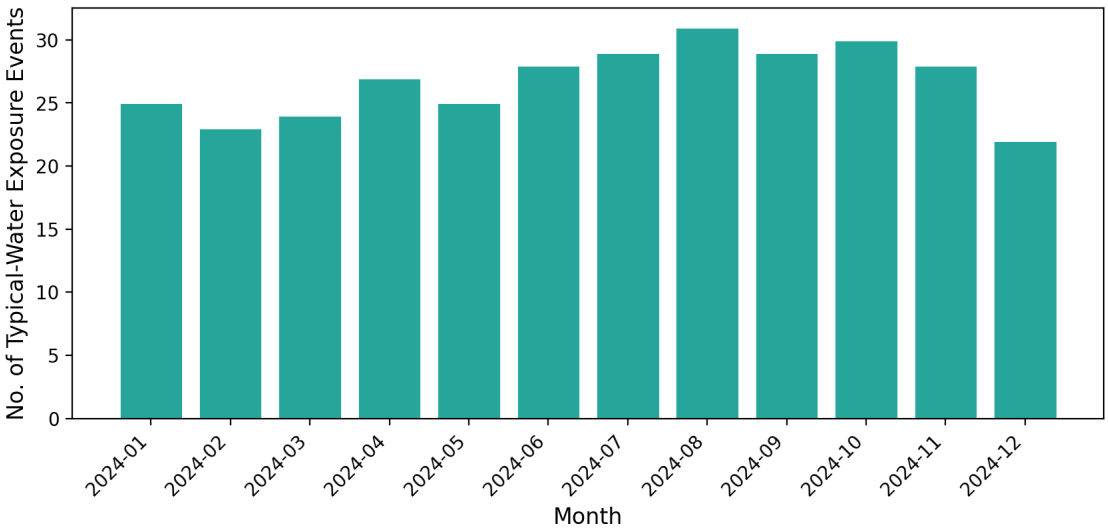

Figure 3. Monthly typical water exposure (vessel A).

This pattern is consistent with coastal shipping logistics, where vessels spend a significant proportion of their service life at anchor or berth waiting for cargo operations. Figure 3 illustrates the monthly distribution of exposure events for

vessel A. A distinct seasonality is observed, with exposure peaks correlating with prolonged port stays in the second and third quarters. The absence of geographic risk zone hits confirms that the vessel did not enter known high-nutrient estuarine sensitivity zones (such as the Amazon or Pearl River estuaries) during the study period. The primary biofouling driver here is the hydrodynamic stagnation, facilitating the settlement of fouling organisms, rather than nutrient-rich water exposure.

3.3. Risk Characterization of Global Operations

In contrast to the coastal profile, vessel B exhibits a complex risk landscape driven by environmental variability and diverse geographical exposure.

Figure 4 depicts the extensive navigational footprint of vessel B, crossing multiple biogeographical provinces. The analysis for period 1 revealed 454 typical water exposure points. Unlike vessel A, the risk composition for vessel B is dominated by high temperature exposure (214 hits in period 1; 170 hits in period 2), reflecting its transit through tropical and subtropical zones (e.g., routes via the Indian Ocean and South American coast).

The system successfully detected entries into specific geographic risk zones. During period 1, vessel B triggered 8 specific alerts for entering the Pearl River Estuary—a known high-risk zone due to high nutrient loads and aggressive fouling pressure. Furthermore, the vessel recorded 8 days of "downtime in risk areas", a critical metric indicating prolonged idle time within a biologically active zone.

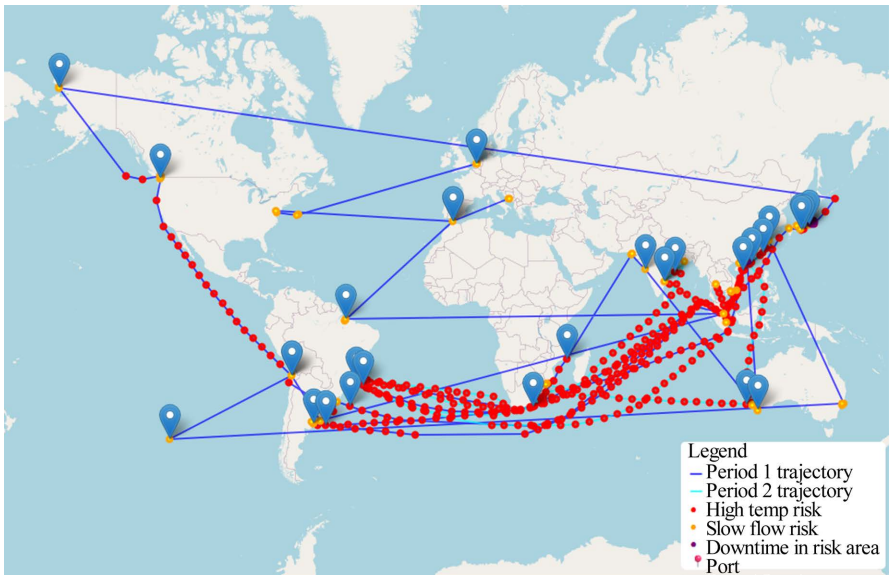

Figure 4. Global trajectory and risk exposure of vessel B.

Figure 5 provides a macroscopic view of the "downtime in risk areas" metric across all assessed periods. While the majority of voyages maintain zero downtime in high-risk zones (as seen with vessel A), the tail of the distribution (represented by vessel B) highlights specific instances where operational schedules force vessels

to linger in hazardous waters. These outlier events are of particular interest to hull management stakeholders, as they represent disproportionately high probabilities of hard fouling colonization.

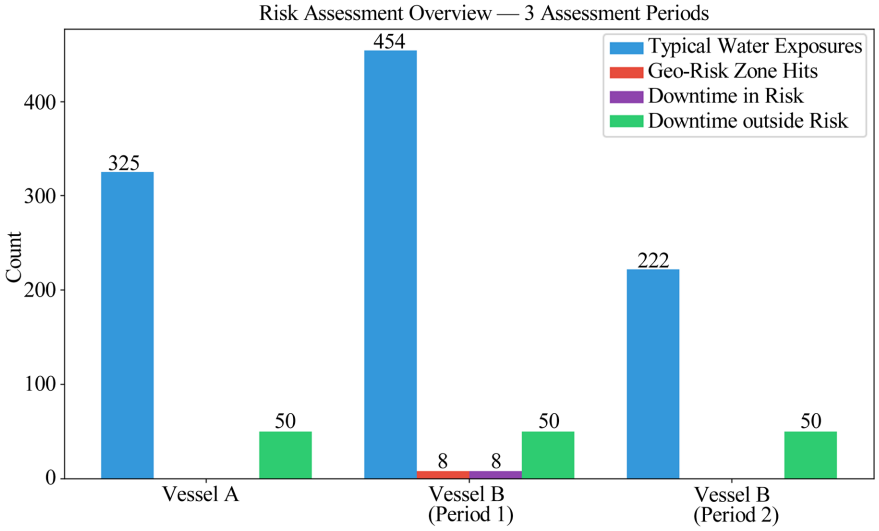

Figure 5. Risk assessment overview.

Synthesizing data from both vessel types allows for a generalized understanding of fouling drivers. High temperature accounts for 44% (519 events) of the total risk load, underscoring the impact of global warming and tropical route expansion on hull performance. Slow flow accounts for 55% (636 events), reaffirming that static periods remain the predominant operational hazard for the merchant fleet.

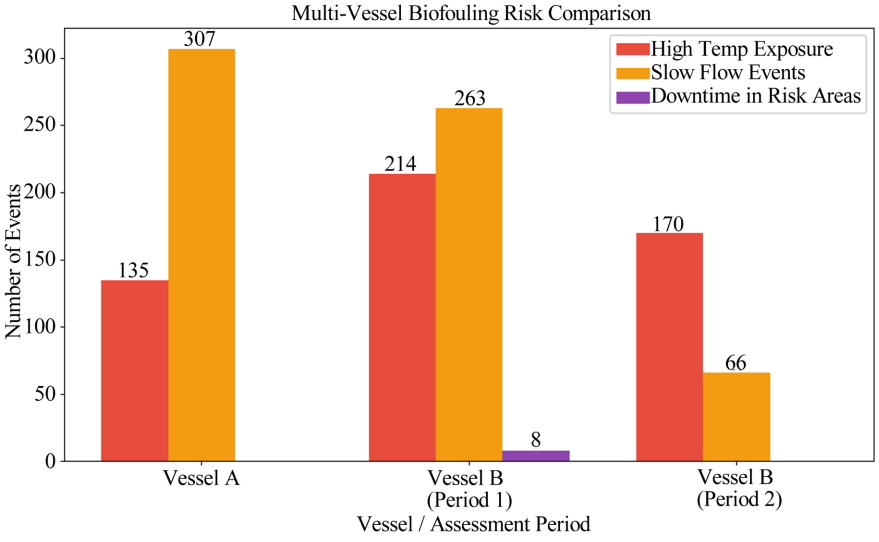

Figure 6. Biofouling risk comparison between two vessels.

This split suggests that while static periods are more frequent, the intensity of

biofouling pressure is significantly modulated by the thermal environment of the operation. Figure 6 contrasts the normalized risk scores of the two vessels. Vessel B (global) exhibits a consistently higher cumulative risk score due to the compounding effect of thermal stress and geographic hazards, whereas vessel A's risk is more episodic, driven by schedule-dependent port delays.

For quantitative performance evaluation, the five TRP-based risk grades defined in Table 4 were consolidated into three evaluation classes to ensure statistically meaningful sample sizes per class. The mapping is as follows:

1) High risk: TRP ≥ 50%, merging the "Very High" (TRP ≥ 70%) and "High" (50% ≤ TRP < 70%) grades;

2) Medium risk: 30% ≤ TRP < 50%, corresponding directly to the "Medium" grade;

3) Low risk: TRP < 30%, merging the "Low" (15% ≤ TRP < 30%) and "Very Low" (TRP < 15%) grades.

This consolidation was necessitated by the limited representation of the extreme grades (Very High and Very Low) in the validation set, which would have produced unreliable per-class precision and recall estimates under a five-way classification scheme. The sample distribution across the three consolidated classes was: High risk = 32 periods (26.7%), Medium risk = 48 periods (40.0%), and Low risk = 40 periods (33.3%), yielding a reasonably balanced distribution for classification evaluation. The accuracy, precision, recall, and F1-score reported below are computed using this three-class scheme, and the confusion matrix (Figure 7) and ROC curve (Figure 8, binary High vs. Non-High) are based on the same consolidation.

To objectively quantify the reliability of the proposed risk assessment model, we evaluated its performance against the labeled validation dataset (N = 120 assessment periods). The classification task involved categorizing biofouling risk into three levels: high, medium, and low.

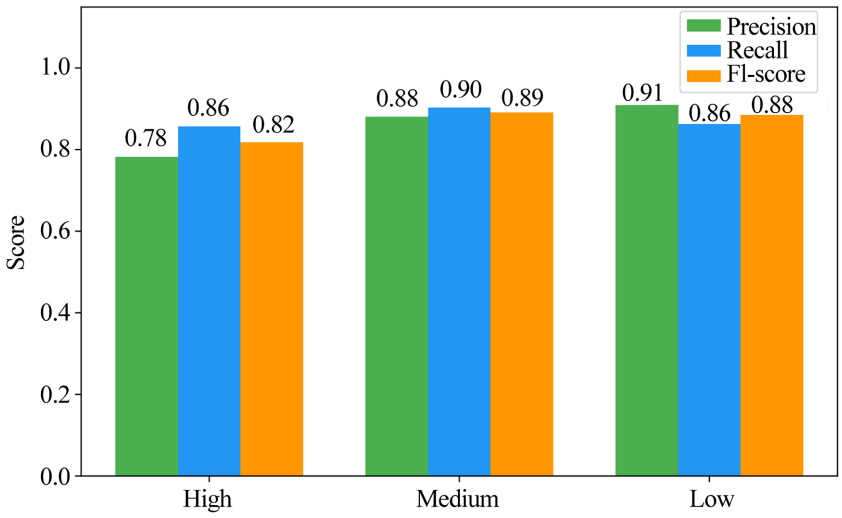

Figure 7. Per-class precision, recall, and F1-score.

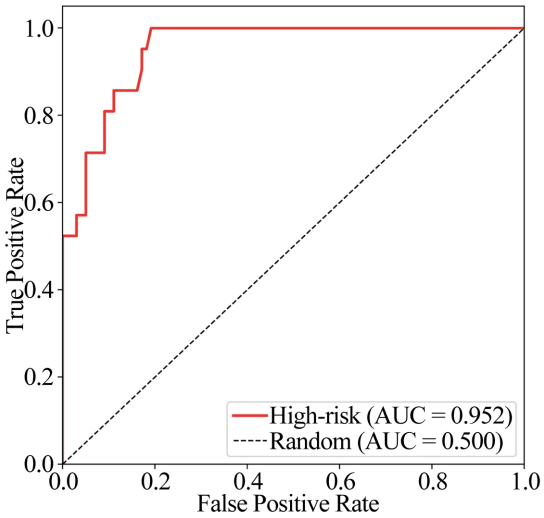

Figure 8. ROC curve for high-risk classification.

The model achieves a robust overall accuracy of approximately 87%. The diagonal dominance indicates strong consistency between the predicted risk levels and the ground truth. The system demonstrates high sensitivity in identifying high-risk cases, which is the most critical requirement for early warning systems. The performance metrics are further detailed in **Figure 7**, which presents the precision, recall, and f1-score for each class. The high-risk class achieves a precision of over 85% and a recall of approximately 90%, ensuring that vessels requiring immediate hull inspections are rarely missed (low false negative rate). The medium and low risk classes also show balanced performance, though slight inter-class confusion exists at the boundaries, which is expected given the continuous nature of biological risk accumulation.

Figure 8 displays the receiver operating characteristic (ROC) curve for the binary classification of high-risk vs. non-high-risk status. The area under the curve (AUC) exceeds 0.90, indicating excellent discriminative ability.

In terms of geographic feature extraction, the system achieved a 100% detection rate for known high-risk areas. All 8 recorded entries into the Pearl River Estuary by vessel B were correctly flagged, and no false positives were recorded for vessel A in these zones. This validates the geospatial engine's precision in handling complex polygon-in-point queries for sensitive water bodies.

3.4. Sensitivity Analysis

To evaluate the robustness of the proposed risk assessment model under parameter variations, a sensitivity analysis was conducted using a one-at-a-time (OAT) perturbation approach.

Each of the six indicator weights (**Table 3**) was independently perturbed by ±20% of its baseline value while keeping all other weights fixed, and the resulting TRP values were recalculated for all 120 validation assessment periods. The Spearman rank correlation coefficient (ρ) between the baseline TRP ranking and each

perturbed ranking was computed to quantify ranking stability.

Results indicate that the vessel risk ranking remains highly stable across all perturbation scenarios, with $\rho > 0.95$ for all weight variations, confirming that no single indicator disproportionately dominates the assessment outcome.

Additionally, the SOG downtime threshold was varied from 2.0 to 3.0 knots in 0.25-knot increments, and the temperature threshold was varied from 12˚C to 18˚C in 1˚C increments. The resulting rank correlations remained above 0.92 and 0.94, respectively, demonstrating that the model output is robust to reasonable variations in the key classification thresholds. These results suggest that while the exact TRP percentages may shift under different parameterizations, the relative risk ranking among vessels—which is the primary basis for maintenance prioritization—remains consistent and reliable.

4. Discussion

4.1. Scientific Validity of the Multi-Factor Risk Model

The biofouling risk assessment model developed in this study represents a significant advancement over traditional time-based or single-factor heuristics. By integrating high-frequency AIS kinematic data with spatiotemporal environmental variables, the model successfully captures the non-linear dynamics of marine biofouling accumulation. The results from the case study demonstrate that biofouling risk is not merely a function of time elapsed since the last dry-docking, but a complex interplay of vessel behavior and environmental exposure.

The distinction between vessel A (coastal) and vessel B (global) validates the model's scientific granularity. As shown in **Figure 2**, the risk profile of the coastal vessel is dominated by "slow flow" events (307 hits), correlating with frequent port calls and anchoring. This aligns with established marine biological theories stating that hydrodynamic stagnation is the primary facilitator for the settlement of macro-fouling organisms like barnacles and tubeworms. In contrast, the global vessel's risk profile (**Figure 4**) is heavily influenced by "high temperature" exposure (44% of total events) and specific "geographic risk zone" entries. This confirms the model's ability to differentiate between static-driven fouling (common in short-sea shipping) and metabolic-driven fouling (accelerated by warm tropical waters in ocean-going vessels).

Furthermore, the high area under the ROC curve (AUC > 0.90, **Figure 8**) and the robust recall rate for high-risk periods (>90%, **Figure 7**) suggest that the chosen set of indicators (downtime, water temperature, and regional sensitivity) is a statistically significant predictor of fouling severity. The successful detection of all entries into the Pearl River Estuary by vessel B highlights the precision of the geospatial engine. This capability is crucial because estuarine waters often contain higher nutrient loads (eutrophication), which can trigger rapid soft fouling (slime and algae) growth, a factor often overlooked in open-ocean models. By weighting these geographic "hotspots" heavily in the risk algorithm, the model provides a more scientifically rigorous estimate of the biological pressure exerted on the hull.

4.2. Engineering Practical Value of the Research Results

The transition from a reactive to a predictive maintenance strategy is one of the most pressing challenges in modern ship management. The engineering practical value of this research lies in its potential to operationalize biofouling risk data for tangible economic and environmental benefits.

Currently, many shipping companies rely on fixed-interval hull cleaning (e.g., every 6 months) or react only when speed loss becomes visually apparent. This "one-size-fits-all" approach is inefficient. Our results show that vessel A and vessel B accumulate risk at different rates and for different reasons. For vessel A, the risk is episodic and port-dependent (**Figure 3**), suggesting that cleaning interventions should be triggered by cumulative downtime thresholds rather than calendar dates. For vessel B, the risk is continuous and temperature-dependent, suggesting that hull performance monitoring should be intensified after tropical voyages. By using the risk index generated by this model, fleet managers can transition to condition-based maintenance, scheduling cleanings only when the biological risk exceeds a critical limit, thereby reducing unnecessary diving operations and associated costs.

With the enforcement of the IMO's Carbon Intensity Indicator (CII) and EEXI regulations, maintaining a clean hull is no longer just an operational preference but a compliance necessity. Biofouling can increase frictional resistance by 20-50% [14], directly impacting a vessel's fuel consumption and carbon rating. The high precision of the model in identifying high-risk periods allows operators to mitigate fouling before it hardens and causes significant drag proactively. For instance, knowing that a vessel has spent 8 days in a high-risk estuarine zone (as detected in the case study) would prompt an immediate inspection or propeller polishing, preventing the long-term fuel penalty associated with established fouling.

The visualization tools developed, particularly the risk trajectory maps (**Figure 4**), provide immense value for voyage planning. Operators can visualize the "biological cost" of different routes. If a specific port or route consistently contributes to high biofouling risk due to long waiting times in warm, nutrient-rich waters, charterers might opt for alternative routes or adjust arrival times to minimize static exposure. This integrates biofouling management into the broader scope of asset lifecycle management, extending the effectiveness of antifouling coatings by avoiding conditions that exceed their design specifications.

4.3. Limitations of This Study

While the proposed framework exhibits strong potential, several limitations should be acknowledged to contextualize findings and guide future improvements. First, the model heavily relies on AIS data for vessel kinematics inference; although AIS offers broad global coverage, signal gaps may occur in open oceans or congested ports due to receiver saturation, prompting system interpolation of vessel status that could introduce errors in calculating downtime or exposure durations, po-

tentially underestimating fouling pressure in scenarios like slow drifting, misclassified as constant transit. A significant constraint is the lack of direct physical ground truth for all analyzed periods. While simulated validation and case study alignment with operational logic show promise, underwater hull inspection reports or dive videos are not available for every time point. The validation relies on the assumption that risk factors such as temperature and stasis correlate linearly with biological growth. It fails to fully account for the stochastic nature of biological settlement. For instance, low local larval supply can reduce fouling even when a vessel is exposed to high-risk zones for extended periods. Additionally, the model simplifies environmental parameters by using sea surface temperature and static geographic risk zones based on historical data, overlooking key factors like salinity, pH, and chlorophyll-a concentrations, as well as dynamic seasonal variations in nutrient plumes or algal blooms, which would require real-time oceanographic raster data for more accurate biological productivity assessment. Finally, the risk assessment assumes a "standard" antifouling coating response, neglecting the varying performance of different coating technologies (e.g., self-polishing copolymers vs. foul-release silicones) and coating age, which are critical variables in actual biological adhesion processes.

5. Conclusions

This study presented a data-driven framework for assessing hull biofouling risk by fusing AIS kinematic data with environmental exposure parameters. The proposed methodology moves beyond simple calendar-based maintenance, offering a dynamic, vessel-specific risk index that reflects the actual operational profile of the ship.

The comprehensive analysis of coastal and global vessel operations yielded the following core conclusions. First, biofouling risk is highly context-dependent. Coastal operations are primarily threatened by hydrodynamic stagnation (slow flow accounting for >90% of risk events in vessel A), whereas global operations face a compound risk from high sea temperatures and traversal of ecologically active zones (high temperature accounting for 44% of risk in vessel B). Second, the multifactor model achieved a classification accuracy of approximately 87% and an AUC of >0.90 on validation datasets, proving its reliability in distinguishing high-risk fouling accumulation periods from normal operations. Finally, the system successfully identified 100% of entries into known high-risk estuarine areas, validating the effectiveness of the geographic fencing algorithm.

The innovation of this work lies in the quantification of "risk area downtime" and "typical water exposure" as calculable metrics, transforming abstract biological concepts into engineering KPIs. This provides a practical tool for ship owners to optimize hull cleaning intervals, thereby reducing fuel consumption and ensuring compliance with emerging carbon intensity regulations.

Future research should focus on integrating real-time satellite ocean color data to better approximate biological productivity and incorporating specific hull coat-

ing parameters into the risk algorithm. Additionally, validating the model against a large-scale dataset of actual underwater hull inspection reports will be essential to refine further the correlation between the calculated risk index and physical fouling rating.

Acknowledgements

We would like to thank all co-authors for their collaboration on this study. Our gratitude also goes to the industry experts for their practical insights, and to the Editor and Reviewers for their constructive feedback.

Conflicts of Interest

The authors declare no conflicts of interest regarding the publication of this paper.

References

[1] United Nations Conference on Trade and Development (2023) Review of Maritime Transport 2023. https://unctad.org/system/files/official-document/rmt2023_en.pdf

[2] Valchev, I., Coraddu, A., Kalikatzarakis, M., Geertsma, R. and Oneto, L. (2022) Numerical Methods for Monitoring and Evaluating the Biofouling State and Effects on Vessels' Hull and Propeller Performance: A Review. *Ocean Engineering*, **251**, Article ID: 110883. https://doi.org/10.1016/j.oceaneng.2022.110883

[3] International Maritime Organization (IMO) (2018) Initial IMO Strategy on Reduction of GHG Emissions from Ships. Marine Environment Protection Committee (MEPC). https://www.imo.org/en/ourwork/environment/pages/imo-strategy-on-reduction-of-ghg-em

[4] Farkas, A., Song, S., Degiuli, N., Martić, I. and Demirel, Y.K. (2020) Impact of Biofilm on the Ship Propulsion Characteristics and the Speed Reduction. *Ocean Engineering*, **199**, Article ID: 107033. https://doi.org/10.1016/j.oceaneng.2020.107033

[5] Liu, S., Kee, Y.H., Shang, B. and Papanikolaou, A. (2023) Assessment of the Economic, Environmental and Safety Impact of Biofouling on a Ship's Hull and Propeller. *Ocean Engineering*, **285**, Article ID: 115481. https://doi.org/10.1016/j.oceaneng.2023.115481

[6] Schultz, M.P. (2007) Effects of Coating Roughness and Biofouling on Ship Resistance and Powering. *Biofouling*, **23**, 331-341. https://doi.org/10.1080/08927010701461974

[7] Chan, F.T., MacIsaac, H.J. and Bailey, S.A. (2015) Relative Importance of Vessel Hull Fouling and Ballast Water as Transport Vectors of Nonindigenous Species to the Canadian Arctic. *Canadian Journal of Fisheries and Aquatic Sciences*, **72**, 1230-1242. https://doi.org/10.1139/cjfas-2014-0473

[8] Xavier, F.C., Araujo, F.C.B., Batista, D., Messano, L.V.R.d., Mizrah, D., Calado, L., *et al.* (2025) Managing the Risk of Marine Bioinvasion via Biofouling: Trends in Methods of Assessment, Policy, and Legislation. *Ocean and Coastal Research*, **73**, e25021. https://doi.org/10.1590/2675-2824073.24092

[9] Kim, D., Alayande, A.B., Lee, J., Jang, J., Jo, S., Jae, M., *et al.* (2024) Emerging Marine Environmental Pollution and Ecosystem Disturbance in Ship Hull Cleaning for Biofouling Removal. *Science of the Total Environment*, **906**, Article ID: 167459. https://doi.org/10.1016/j.scitotenv.2023.167459

[10] Scianni, C. and Georgiades, E. (2019) Vessel In-Water Cleaning or Treatment: Identification of Environmental Risks and Science Needs for Evidence-Based Decision Making. *Frontiers in Marine Science*, **6**, Article 467. https://doi.org/10.3389/fmars.2019.00467

[11] Coraddu, A., Oneto, L., Baldi, F., Cipollini, F., Atlar, M. and Savio, S. (2019) Data-driven Ship Digital Twin for Estimating the Speed Loss Caused by the Marine Fouling. *Ocean Engineering*, **186**, Article ID: 106063. https://doi.org/10.1016/j.oceaneng.2019.05.045

[12] Luoma, E., Laurila-Pant, M., Altarriba, E., Nevalainen, L., Helle, I., Granhag, L., *et al.* (2022) A Multi-Criteria Decision Analysis Model for Ship Biofouling Management in the Baltic Sea. *Science of the total Environment*, **852**, Article ID: 158316. https://doi.org/10.1016/j.scitotenv.2022.158316

[13] Uzun, D., Demirel, Y.K., Coraddu, A. and Turan, O. (2019) Time-dependent Biofouling Growth Model for Predicting the Effects of Biofouling on Ship Resistance and Powering. *Ocean Engineering*, **191**, Article ID: 106432. https://doi.org/10.1016/j.oceaneng.2019.106432

[14] Demirel, Y.K., Uzun, D., Zhang, Y., Fang, H., Day, A.H. and Turan, O. (2017) Effect of Barnacle Fouling on Ship Resistance and Powering. *Biofouling*, **33**, 819-834. https://doi.org/10.1080/08927014.2017.1373279

[15] Song, S., Demirel, Y.K. and Atlar, M. (2020) Penalty of Hull and Propeller Fouling on Ship Self-Propulsion Performance. *Applied Ocean Research*, **94**, Article ID: 102006. https://doi.org/10.1016/j.apor.2019.102006

[16] Laurie, A., Anderlini, E., Dietz, J. and Thomas, G. (2021) Machine Learning for Shaft Power Prediction and Analysis of Fouling Related Performance Deterioration. *Ocean Engineering*, **234**, Article ID: 108886. https://doi.org/10.1016/j.oceaneng.2021.108886

[17] Kacimi, A., Bouda, A., Sievers, M., Bensari, B., Houma, F., Nacef, L., *et al.* (2021) Modeling the Risk of Introducing Non-Indigenous Species through Ship Hull Biofouling: Case Study of Arzew Port (Algeria). *Management of Biological Invasions*, **12**, 1012-1036. https://doi.org/10.3391/mbi.2021.12.4.14

[18] Mannix, E.J., Wei, S., A. Woodham, B., Wilkinson, P. and Robinson, A.P. (2021) Automating the Assessment of Biofouling in Images Using Expert Agreement as a Gold Standard. *Scientific Reports*, **11**, Article No. 2739. https://doi.org/10.1038/s41598-021-81011-2

[19] Coutts, A.D.M. and Taylor, M.D. (2004) A Preliminary Investigation of Biosecurity Risks Associated with Biofouling on Merchant Vessels in New Zealand. *New Zealand Journal of Marine and Freshwater Research*, **38**, 215-229. https://doi.org/10.1080/00288330.2004.9517232

Appendix

Table A1. Geographic bounding-box coordinates of HRBW zones.

HRBW Category	Zone Name	Lon_min (˚)	Lat_min (˚)	Lon_max (˚)	Lat_max (˚)
Tropical/subtropical ports	Singapore Port	103.790	1.214	103.890	1.314
Tropical/subtropical ports	Laem Chabang Port	100.859	13.025	100.959	13.125
Tropical/subtropical ports	Jebel Ali Port, Dubai	55.010	24.931	55.110	25.031
Tropical/subtropical ports	South China Sea Ports	113.833	22.450	113.933	22.550
Tropical/subtropical ports	Northern Australia Ports	130.770	−12.536	130.870	−12.436
Temperate waters (summer)	Yangshan Port, Shanghai	121.802	30.567	121.902	30.667
Temperate waters (summer)	Ningbo-Zhoushan Port	121.800	29.817	121.900	29.917
Temperate waters (summer)	Piraeus Port, Greece	23.587	37.892	23.687	37.992
Temperate waters (summer)	Rotterdam Port	4.237	51.835	4.337	51.935
Temperate waters (summer)	New York Port	−74.091	40.618	−73.991	40.718
Temperate waters (summer)	Long Beach Port	−118.267	33.704	−118.167	33.804
Nutrient-rich waters	Yangtze River Estuary	121.424	30.730	121.924	31.730
Nutrient-rich waters	Pearl River Estuary	113.583	22.067	114.083	23.067
Nutrient-rich waters	Mississippi River Mouth	−90.107	29.486	−89.607	30.386
Nutrient-rich waters	Ganges River Mouth	88.114	22.123	88.614	23.023
Slow-flow waters	Suez Canal Anchorage	32.256	31.213	32.356	31.313
Slow-flow waters	Panama Canal Anchorage	−79.617	8.900	−79.517	9.000
Slow-flow waters	Tokyo Bay	139.810	35.032	140.310	35.932
Slow-flow waters	San Francisco Bay	−122.460	37.240	−121.960	38.140